

Studies of one- and two-hole states in the 2D t - J model via series expansions

C.J. Hamer*, Zheng Weihong[†], and J. Oitmaa[‡]

School of Physics, The University of New South Wales, Sydney, NSW 2052, Australia.

(June 26, 1998)

Abstract

We study one and two hole properties of the t - J model at half-filling on the square lattice using series expansion methods at $T = 0$. The dispersion curve for one hole excitations is calculated and found to be qualitatively similar to that obtained by other methods, but the bandwidth for small t/J is some 20% larger than given previously. We also obtain the binding energy and dispersion relation for two hole bound states. The lowest bound state as t/J increases is found to be first d -wave, and then p -wave, in accordance with predictions based upon the Kohn-Luttinger effect. We also make a similar study for the t - J_z model.

PACS Indices: 71.27.+a, 71.10Fd

I. INTRODUCTION

Models of strongly correlated electrons in two dimensions have been much studied in recent years as part of a search for a minimal model of the high- T_c superconducting cuprates, and other fascinating new antiferromagnetic systems [1–3]. The t - J model, defined by the Hamiltonian

$$H = -t \sum_{\langle ij \rangle, \sigma} P(c_{i,\sigma}^\dagger c_{j,\sigma} + c_{j,\sigma}^\dagger c_{i,\sigma})P + J \sum_{\langle ij \rangle} (\mathbf{S}_i \cdot \mathbf{S}_j - \frac{1}{4} n_i n_j) \quad (1)$$

has become a generic model for mobile electrons/holes in doped antiferromagnets. In this expression the $c_{i,\sigma}^\dagger$, $c_{i,\sigma}$ are the usual electron creation and destruction operators, \mathbf{S}_i are the electron spin operators and the sum is over nearest neighbors pairs. P is a projection operator which ensures that doubly occupied states are excluded.

The t - J model originally was derived [4] as the strong correlation limit of the Hubbard model, with $J = 2t^2/U$, but it is now generally treated as an effective Hamiltonian in its own right, with t and J independent parameters. For the cuprates it is estimated [5] that $t/J \simeq 3$, which is well outside the region of validity of the Hubbard mapping. An independent “derivation” of the t - J model as an effective Hamiltonian for the cuprates has been presented by Zhang and Rice [6].

At exactly half-filling (one electron per site) the kinetic term vanishes because of the single-occupancy restriction and the model reduces to an antiferromagnetic insulator. It is known from a variety of numerical and analytic calculations [7] that this model, on the square lattice, has nonzero long range antiferromagnetic (Néel) order, reduced by strong quantum fluctuations. Removal of a small number of electrons (by doping) will allow mobility of holes and will reduce the antiferromagnetic order. The physics of a small number of holes in a dynamic antiferromagnetic background remains a challenging problem. Previous studies of the t - J model at $T = 0$ have used a variety of approaches. Exact diagonalization methods have been used extensively on clusters up to 32 sites [8–11], but suffer from substantial finite-size corrections and an inability to treat extended excitations. Green’s function Monte Carlo calculations have been performed for larger lattices, up to 8×8 [12], and show, for example, a significant decrease of the two-hole binding energy with increasing lattice size. A variety of variational approaches and analytic many body methods have also been employed [13–19].

The picture that emerges from this body of work is roughly as follows. For one hole the ground state energy is given by

$$\epsilon_{1h}/t \simeq -3.2 + 2.8(J/t)^{0.73} \quad (2)$$

where the coefficients are approximate numerical estimates. The dispersion curve for 1-hole states is qualitatively similar from different methods, with minima at $(\pi/2, \pi/2)$ and equivalent points. The bandwidth from the largest diagonalizations scales as

$$W/t \simeq -0.33 + 2.04(J/t)^{0.64} \quad (3)$$

where the coefficients are again estimates and are not known with great precision. The spectral function for 1-hole states has been calculated [10] and shows a clear quasiparticle peak, together with a continuum at higher energies. For two holes the binding energy,

spectral function and pair susceptibility have been computed. The results support the existence of a bound state with $S = 0$ and d-wave symmetry for $J > J_c$, with $J_c \simeq 0.3t$ although not all methods agree and this is still controversial. The dispersion curve for two-hole bound states is also of interest – to our knowledge the only calculation of this is due to Eder [14].

The aim of the present work is to study the physics of one-hole and two-hole states in the half-filled t - J model at zero temperature via linked-cluster series expansions. This approach has been developed extensively in recent years by our group [20–22] and others [23–25]. Most of the applications to date have been to spin systems, although we have included fermions in lattice gauge calculations. Shi and Singh [26] have used this approach to study the Hubbard model at half filling, via an expansion about an additional Ising term included in the Hamiltonian. For completeness we also mention the use of high-temperature expansions to study the t - J model [27,28]. The present work of course addresses different questions which cannot be probed by high-temperature series.

The plan of the paper is as follows. In Sec. II, the series expansion method is briefly reviewed, and the results for one-hole properties of the t - J model are presented. In Sec. III, we study the dispersion relation and the binding energy for two-hole bound states. In Sec. IV, we study the one-hole and two-hole properties of the t - J_z model. Sec. V is devoted to a summary and discussion.

II. ONE-HOLE PROPERTIES

The series expansion method is based on a linked cluster formalism associated with standard Rayleigh-Schrödinger perturbation theory.

The ground state energy E_0^N for a lattice of N sites can be written as a sum over all connected clusters $\{\alpha\}$ as

$$E_0^N = \sum_{\alpha} C_{\alpha}^N \epsilon_{\alpha} \quad (4)$$

where C_{α}^N is a geometrical embedding factor and ϵ_{α} is the “cumulant energy” of cluster α . The same formula can be used for the energy of any particular cluster β

$$E_0^{\beta} = \sum_{\alpha} C_{\alpha}^{\beta} \epsilon_{\alpha} \quad (5)$$

where the sum is now over all sub-clusters embeddable in β . The cluster energy is calculated perturbatively, then the cumulant energies are obtained iteratively from Eq. (5) and substituted into Eq. (4) to obtain the final series. The formalism for excited states, needed to compute the dispersion curves, is a little more complex [25].

We introduce an Ising spin anisotropy

$$\begin{aligned} J(\mathbf{S}_i \cdot \mathbf{S}_j - \frac{1}{4}n_in_j) &\rightarrow J_z(S_i^z S_j^z - \frac{1}{4}n_in_j) + J_{xy}(S_i^x S_j^x + S_i^y S_j^y) \\ &= J_z[(S_i^z S_j^z - \frac{1}{4}n_in_j) + x(S_i^x S_j^x + S_i^y S_j^y)] \end{aligned} \quad (6)$$

where $x = J_{xy}/J_z$, and rewrite the Hamiltonian for the t - J model as

$$H/J_z = H_0 + xV \quad (7)$$

with

$$H_0 = \sum_{\langle ij \rangle} (S_i^z S_j^z - \frac{1}{4} n_i n_j) + r \sum_i (-1)^i S_i^z \quad (8)$$

$$V = -\frac{t}{J_{xy}} \sum_{\langle ij \rangle, \sigma} P(c_{i,\sigma}^\dagger c_{j,\sigma} + c_{j,\sigma}^\dagger c_{i,\sigma}) P + \sum_{\langle ij \rangle} (S_i^x S_j^x + S_i^y S_j^y) - r \sum_i (-1)^i S_i^z \quad (9)$$

with a staggered z -field of strength r to improve convergence [26]. This term vanishes in the total Hamiltonian in the isotropic exchange limit $x \rightarrow 1$. The Ising part of the exchange, H_0 , forms the unperturbed Hamiltonian while the perturbation V includes both the hole hopping terms and transverse spin fluctuations. The original Hamiltonian for the t - J model is recovered in the limit $x = 1$ (i.e. $J = J_z = J_{xy}$). We expect the series expansion to give more reliable results in the small t/J region, where the perturbation V is less important.

We directly compute the series for the ground state energy difference between the system with one (or two) hole(s) and the system with no hole. Two types of series can be obtained in this way. By fixing $y \equiv t/J_{xy}$ and r we can compute series in the single variable x up to order L (where L is typically of order 11-13),

$$E/J_z = \sum_{i=0}^L c_i(y, r) x^i \quad (10)$$

We refer to these as x -series. Extrapolation to $x = 1$ is carried out by standard Padé approximant or integrated differential approximant methods [29]. In the other approach we keep both x and t/J_z as expansion parameters and obtain double series of the form

$$E/J_z = \sum_{ij} d_{ij}(r) (t/J_z)^i x^j \quad (11)$$

where the coefficients d_{ij} are computed up to order $i + j \leq L$. Extrapolation to $x = 1$ then yields a series in t/J ,

$$E/J = \sum_i e_i (t/J)^i \quad (12)$$

which we refer to as a t -series.

We first consider states with one hole, which may exist either on the up-sublattice (A) or the down-sublattice (B), where the up and down sublattice are represented in Fig. 1(a) by open and full circles, respectively. Here (e_x, e_y) are the usual primitive translation vectors. The unperturbed wave function for the zero-momentum spin-up state is taken to be

$$|\Psi\rangle = \sum_{i \in A} c_{i,\uparrow} |N\rangle \quad (13)$$

where $|N\rangle$ is the classical Néel state. Now a hole in the up (down) sublattice can never transform into a single hole in the down (up) sublattice, since the Hamiltonian conserves

the total spin $\sum_i S_i^z$; so that we should choose $(e_{x'}, e_{y'})$ shown in Fig. 1(a) as the primitive translation vectors, rather than (e_x, e_y) . The unit vectors $(e_{x'}, e_{y'})$ are those of the antiferromagnetic bipartite lattice. The Brillouin zones in reciprocal space corresponding to these different choices are shown in Fig. 1(b). Most previous calculations, however, have used (e_x, e_y) as unit vectors (corresponding to (k_x, k_y) in momentum space), instead of $(e_{x'}, e_{y'})$, so we will also conform to this convention (and set a to one) unless it is specified otherwise.

For momentum $\mathbf{k} = 0$ we obtain the energy to order $L = 13$, involving 8739 distinct clusters containing up to 13 sites. For $\mathbf{k} \neq 0$ it is necessary to distinguish between clusters having different spatial orientation. We expand the energy to order $L = 11$, involving 23546 clusters with up to 11 sites. The series coefficients for $y = 0.5$ at fixed momentum $(k_x, k_y) = (\pi/2, \pi/2)$ and different r are listed in Table I, where we can see the series converges best around $r = 2$. The extrapolations of these series by using the integrated differential approximant methods are shown in Figure 2, where we can see that at $x = 1$, the extrapolations from different r series agree with each other very well, while the case $r \simeq 2$ gives the smallest error bar. In Table II, we list the full spectrum series for $y = 0.5$ and $r = 0$. The other coefficients are too lengthy to publish but can be supplied on request.

In Figure 3 we show the energy of a one-hole state for \mathbf{k} along symmetry directions in the Brillouin zone, for various ratios t/J obtained from x -series. The lowest energy occurs at $(k_x, k_y) = (\pi/2, \pi/2)$ and equivalent points. This result, and the overall shape of the one-hole dispersion curve are in very good agreement with previous work [13,30,31,10,11]. We note that the symmetry and the redundant information evident in Fig. 3 are the results of choosing a Brillouin zone which is two times too big. If we choose $(k_{x'}, k_{y'})$ as defining the bipartite Brillouin zone, the corresponding dispersion relation along symmetry directions in the Brillouin zone is shown in Fig. 4. Figure 5 shows the one-hole bandwidth, $W = E(0,0) - E(\pi/2, \pi/2)$, as a function of J/t , compared with results from other approaches. For J/t around 0.5 our results agree well with other work, but for large J/t our result is significantly larger than that obtained by Martinez and Horsch [31]. Also we found a peak value of $W/t \simeq 1.15$ at $J/t \simeq 1.25$, rather than $W/t \simeq 1$ at $J/t = 0.8$ as obtained by Martinez and Horsch [31], and Liu and Manousakis [13].

Using the two-variable expansion we obtain the one-hole energy $E(\mathbf{k})$ at some particular values of \mathbf{k} :

$$\begin{aligned} E^{1h}(0,0)/J &= 2.164(2) - 0.655(8)(t/J)^2 - 0.031(5)(t/J)^4 + O[(t/J)^6] \\ E^{1h}(\pi/2, \pi/2)/J &= 2.164(2) - 3.91(4)(t/J)^2 + 9.1(4)(t/J)^4 + O[(t/J)^6] \\ E^{1h}(\pi, 0)/J &= 2.164(2) - 2.68(2)(t/J)^2 + 3.06(4)(t/J)^4 + O[(t/J)^6] \end{aligned} \quad (14)$$

These coefficients are not exact as they involve an extrapolation to $x = 1$. The leading coefficient 2.164(3) can be compared with 2.1552 from a spin wave calculation [32] and 2.193(7) from a Monte Carlo simulation [33].

The bandwidth can be obtained as

$$W/J = 3.26(5)(t/J)^2 - 9.1(4)(t/J)^4 + O[(t/J)^6] \quad (15)$$

This result is also plotted in Figure 5 as a dashed line, and it agrees well at small t/J with that obtained from x -series. The leading coefficient 3.26(5) should be compared with previous calculations giving a value of 2 [31] or 2.6 [34].

III. TWO-HOLE PROPERTIES

In the previous section we developed a series expansion approach to calculate one-hole properties of the t - J model, and showed how reliable quantitative results could be obtained. In the present section we extend this approach to consider states with two holes.

We start from an unperturbed wave-function consisting of two nearest-neighbour holes with opposite spin, and overall momentum \mathbf{k} :

$$|\Psi(\mathbf{k})\rangle = \sum_{i \in A} c_{i,\uparrow} e^{i\mathbf{k} \cdot \mathbf{x}_i} (c_{i-e_x,\downarrow} e^{-ik_x a/2} + c_{i+e_x,\downarrow} e^{ik_x a/2} + c_{i-e_y,\downarrow} e^{-ik_y a/2} + c_{i+e_y,\downarrow} e^{ik_y a/2}) |N\rangle \quad (16)$$

Here again there are two different choices of Brillouin zone possible. One may choose to use a diagonal unit vector of length $a/\sqrt{2}$ (where a is the lattice spacing), which connects the centre points of two adjacent bonds of the original lattice as shown in Fig. 6(a); this corresponds to the large, outer Brillouin zone in Fig. 6(b). This was basically the convention used by Eder [14]. Alternatively, and more correctly, one may choose a diagonal unit vector of length $\sqrt{2}a$, differentiating between the A and B sublattices. This gives rise again to the Brillouin zone of the bipartite lattice, marked as the inner zone in Fig. 6(b). In this second case, there are 4 independent bond states in the unit cell, and one may form linear combinations of them making up the conventional s -, p_x -, p_y - and d -wave states. With the first choice, all these four states are included within one Brillouin zone: the points corresponding to zero-momentum s -, p_x -, p_y - and d -wave states are shown¹ in Fig. 6(b). Then one finds that the different states are related by equations such as

$$E^{2d}(k_x, k_y) = E^{2s}(\pi - k_x, \pi - k_y) \quad (17)$$

(in units where $a/\sqrt{2}$ has been rescaled to one). This relationship is evident in Fig. 19 of Ref. [14].

We have computed series for the two-hole spectrum $E^{2h}(\mathbf{k})$ up to order $L = 11$. This involves 46,440 distinct clusters of up to 12 sites. The x -series coefficients for $y = 0.5$ and $r = 0$ are listed in Table II.

Using the two-variable expansion, after extrapolation to $x = 1$, we obtain the following estimates for the two-hole s -, p - and d -wave pair energy:

$$\begin{aligned} E^{2d}/J &\equiv E^{2h}(0,0)/J = 3.798(2) - 7.66(3)(t/J)^2 + 17.5(5)(t/J)^4 + O[(t/J)^6] \\ E^{2p}/J &\equiv E^{2h}(0,\pi)/J = 3.798(2) - 3.705(10)(t/J)^2 - 4.1(1)(t/J)^4 + O[(t/J)^6] \\ E^{2s}/J &\equiv E^{2h}(\pi,\pi)/J = 3.798(2) - 0.52(3)(t/J)^2 - 1.62(5)(t/J)^4 + O[(t/J)^6] \end{aligned} \quad (18)$$

So the binding energies defined by

$$E_b(\mathbf{k}) \equiv E^{2h}(\mathbf{k}) - 2E^{1h}(\pi/2, \pi/2) \quad (19)$$

for s -, p - and d -wave pair states are:

¹The “ p_x -” and “ p_y -” wave states are degenerate by reflection symmetry. The points marked p_x and p_y in Fig. 6(b) are really linear combinations of the proper p_x and p_y states.

$$\begin{aligned}
E_b^{2d}/J &= -0.529(4) + 0.16(10)(t/J)^2 - 0.7(13)(t/J)^4 + O[(t/J)^6] \\
E_b^{2p}/J &= -0.529(4) + 4.1(1)(t/J)^2 - 22.3(9)(t/J)^4 + O[(t/J)^6] \\
E_b^{2s}/J &= -0.529(4) + 7.3(1)(t/J)^2 - 19.8(9)(t/J)^4 + O[(t/J)^6]
\end{aligned}
\tag{20}$$

The binding energy for $t = 0$ has previously been given as -0.51 by spin wave theory [32], and $-0.58(2)$ by Monte Carlo [33]. Our result is in relatively good agreement but suggests that the Monte Carlo calculations may overestimate the binding energy somewhat.

We have also computed the dispersion curves for the two-hole bound state from x -series, and these are shown in Figure 7, for various small t/J . The minimum occurs at (π, π) (d -wave pair), and the maximum occurs at $(0, 0)$ (s -wave pair), while the energy at $(0, 0)$ is almost unchanged as t/J increases. The curves are quite flat for small t/J , as expected, and develop more structure as t/J increases. The results are broadly similar to those of Eder [14].

The s -, p - and d -wave pair binding energies, obtained from both the x -series and the two-variable expansion as a function of t/J , are shown in Figure 8. Note that for x -series, the extrapolation is done on series for $E_b(\mathbf{k})$, rather than the 1-hole and 2-hole energies individually, because values of these two energies are quite large, while their difference is usually small. The convergence is excellent for small t/J , and we believe our results are very accurate there. The uncertainty increases for larger t . We can see from this figure that as t/J increases from zero, the s -wave binding energy decreases very quickly, and the binding disappears around $t/J \simeq 0.295$. The p -wave binding energy also decreases quickly in the small t/J region, but it turns out to be very flat beyond $t/J \sim 1$, and the binding energy is very small. The d -wave binding energy decreases slightly as t/J increases from zero. Our results are consistent with the d -wave binding disappearing around $t/J \sim 2.5$. Beyond that point, the p -wave state appears to have the lower energy, and remains very weakly bound according to our results.

Figure 8 also shows some other numerical results for the 2-hole binding energy. The solid circles with error bars are GFMC results for the 8×8 lattice obtained by Boninsegni and Manousakis [12], and lie somewhat below our result, though broadly similar in trend: the discrepancy may easily be attributed to a finite-size effect. The solid triangles are the results of a recent 32-site finite-lattice calculation [35]. The open circles are the results of a linear extrapolation in $1/N$ from the finite-lattice data by Chernyshev, Leung and Gooding [35]; but they discuss reasons why such a naive extrapolation is not to be relied on especially at large t/J . The results lie somewhat above our series results for the d -wave binding energy, but again have a broadly similar trend. Chernyshev, Leung and Gooding [35] find that the lowest bound state on the 32-site lattice is a singlet state with $d_{x^2-y^2}$ symmetry.

The apparent cross-over between the p -wave and d -wave bound states came initially as a surprise. But in fact it accords very well with predictions [36,37] based on the Kohn-Luttinger effect. In a repulsive Fermi liquid, pairing in high-angular momentum states can occur due to a singularity in the 2-particle scattering amplitude. This effect was previously believed not to occur in two dimensions, because it does not appear up to second order in perturbation theory; but it was recently shown [36,37] that a singularity does arise at higher order. Chubukov [37] showed that in the dilute limit the effect survives down to $l = 1$ and gives rise to p -wave pairing. He also pointed out that the same effect will occur in an arbitrarily dense Fermi liquid. Both numerical [38] and analytical [39,40] approaches have

shown that at low densities p -wave pairing is dominant for $J/t \ll 1$, d -wave is dominant at $J/t > 1$, and there is a region of s -wave dominance for $J/t \gtrsim 2$. Figure 8 appears to indicate that a similar pattern extends even to the region of half-filling. In fact, the earlier variational calculation² of Eder also shows a crossover between p -wave and d -wave states (Fig. 21 of Ref. [14]) at around $t/J = 2$.

Several theoretical approaches [17–19] have predicted that magnon exchange should give rise to shallow, long-range bound states even at large t/J values. The behaviour of the p -wave state looks consistent with this idea, but not the d -wave state. It is possible that another state (or states) in the d -wave sector could cross over the one we have calculated, and become the lowest energy state at large t/J . Such a crossover could typically imply a square-root singularity in the energy eigenvalue, and the series extrapolation would no longer be valid beyond that point.

IV. T- J_z MODEL

We also study a simplified version of the t - J model, the t - J_z model, which has an Ising rather than a Heisenberg spin interaction

$$H = J_z \sum_{\langle ij \rangle} (S_i^z S_j^z - \frac{1}{4} n_i n_j) - t \sum_{\langle ij \rangle, \sigma} P(c_{i,\sigma}^\dagger c_{j,\sigma} + c_{j,\sigma}^\dagger c_{i,\sigma}) P \quad (21)$$

Here we naturally take the first term in H as the unperturbed Hamiltonian, and the second term as the perturbation, and perform an expansion in t/J_z . This expansion only converges well up to about $t/J_z \sim 2$. To improve the convergence in the large t/J_z region, we can include a staggered z -field of strength r as in the t - J model, and perform the following separation,

$$H/J_z = H_0 + xV \quad (22)$$

where

$$H_0 = \sum_{\langle ij \rangle} (S_i^z S_j^z - \frac{1}{4} n_i n_j) + r \sum_i (-1)^i S_i^z \quad (23)$$

$$V = -\frac{t}{J_z} \sum_{\langle ij \rangle, \sigma} P(c_{i,\sigma}^\dagger c_{j,\sigma} + c_{j,\sigma}^\dagger c_{i,\sigma}) P - r \sum_i (-1)^i S_i^z \quad (24)$$

We then take H_0 as the unperturbed Hamiltonian and V as the perturbation, and perform an expansion in x for fixed values of t/J_z and r . Here again we need to extrapolate the series to $x = 1$.

The series for the one-hole state have been computed up to order 21 (that is, to $(t/J_z)^{21}$ for the Hamiltonian in Eq. (21) or to order x^{21} for the Hamiltonian in Eq. (22)) involving a

²There is a discrepancy between Eder's results and ours, which is due to his omission of the term $-1/4n_i n_j$ in the Hamiltonian.

list of 23546 clusters with up to 11 sites, while the series for the two-hole bound state have been computed up to order 18, involving a list of 23546 clusters up to 11 sites. The final series in t/J_z for the spectrum of the one-hole state and two-hole bound state are listed in Table III.

Fig. 9 shows the one-hole spectrum for some particular values of t/J_z . Here we can see that the shape of the dispersion curve is quite different from that for the t - J model: the lowest energy occurs at $(0, 0)$ rather than $(\pi/2, \pi/2)$ as in the t - J model, and the bandwidth here is about 10 times smaller than that for the t - J model. The minimum one-hole energy as a function of J_z/t is shown in Fig. 10. In the interval $0.2 \leq J_z/t \leq 1$, the minimum one-hole energy can be very well fitted [41,8] as

$$E^{1h}/t = -3.60 + 2.9(J_z/t)^{2/3} + J_z/t \quad (25)$$

where the linear term comes from the $-1/4n_i n_j$ term in the Hamiltonian. This is in good agreement with previous estimates [41,8].

The two-hole dispersion is shown in Fig. 11. We note that the energy at $(0, 0)$ is exactly $7J_z/2$, independent of t , and the energy along path $(\pi, 0)$ (p -wave pair) to (π, π) (d -wave pair) is very flat.

The s -, p - and d -wave binding energies defined by

$$E_b(\mathbf{k}) \equiv E^{2h}(\mathbf{k}) - 2E^{1h}(\mathbf{k} = 0) \quad (26)$$

are shown in Figure 12. We can see from this figure that s -wave binding disappears around $t/J_z \simeq 0.32$. The d -wave binding energies are slightly greater than for p -wave when $t/J_z \lesssim 0.83$, but when $t/J_z \gtrsim 0.83$, the p -wave pair has a greater binding energy than the d -wave, similarly to that found for the full t - J model. Thus the t - J_z model also shows a crossover between d -wave and p -wave bound states, occurring even earlier than in the full t - J model. Again, the earlier variational calculations of Eder showed very similar results (Fig. 12 of Ref. [14]).

The solid points in Figure 12 are the results of a reduced basis diagonalization study on clusters of up to 50 sites by Riera and Dagotto [41]. The trend of these results agrees extremely well with the series estimates, although their estimates lie systematically a little lower. They do not discuss the symmetry of the bound state [41]. They find the binding of the 2-hole state disappears at $J_z/t \simeq 0.183$, or $t/J_z \simeq 5.5$, which agrees very well with our results.

V. CONCLUSIONS

The t - J model on the square lattice has been studied by many workers over the last decade, using a variety of techniques. These methods are all approximate and have uncertain accuracy. Independent confirmation from a variety of approaches increases one's confidence in the results.

We have used the linked-cluster series expansion method to study one and two hole properties of the half-filled t - J and t - J_z models in 2-dimensions at $T = 0$. To our knowledge this is the first time this has been done. Our results for 1-hole and 2-hole states can be summarized as follows:

- The 1-hole dispersion curve has been computed throughout the Brillouin zone, and agrees in shape with previous calculations.
- The minimum for 1-hole dispersion occurs at $(\pi/2, \pi/2)$ and equivalent points, again in agreement with previous work.
- The bandwidth W for the 1-hole dispersion curve of the t - J model has been calculated. At small J/t it agrees with the spin-wave calculations of Martinez and Horsch [31] and Liu and Manousakis [13], but beyond $J/t \simeq 1$ our results lie substantially higher than theirs. We get a peak value of $W/t \simeq 1.15$ at $J/t \simeq 1.25$, rather than $W/t \simeq 1$ at $J/t \simeq 0.8$ as given in previous work.
- We have computed the dispersion curve for 2-hole bound states. To our knowledge this has not been well calculated previously.
- In the limit $t/J = 0$ of the t - J model, we can compare our results for the one-hole and two-hole energy (E^{1h} and E^{2h}), the binding energy (E_b), and the bandwidth for the one-hole state (W) with previous spin-wave [32], Monte Carlo [33] and other calculations.

	This Work	Previous works
E^{1h}/J	2.164(2)	2.155(SW), 2.193(MC)
E^{2h}/J	3.798(2)	3.79436(SW), 3.801(8)(MC)
E_b/J	-0.529(4)	-0.51(SW), -0.58(2)(MC)
W	$3.26(t/J)^2$	$2(t/J)^2$ [31], $2.6(t/J)^2$ [34]

We can see that our results agree very well with other results, except for W , where we find a significantly larger value for the leading coefficient.

- At large t/J , we find a crossover in binding energy between the d -wave and p -wave 2-hole states, for both the t - J and t - J_z models. This phenomenon is likely to arouse some controversy: it certainly needs to be checked by other methods. As supporting evidence, we note the following points:
 - i) The trend of the series results for the t - J_z model agrees very well with numerical calculations of Riera and Dagotto [41];
 - ii) The phenomenon would be in accord with the Kohn-Luttinger effect as predicted by Baranov, Kagan and Chubukov [36,37], and confirmed at low densities [39,38,40]. Chubukov pointed out that the same effect should occur in an arbitrarily dense Fermi liquid.
 - iii) Very much the same phenomenon was observed previously in the variational calculations of Eder [14]. The concordance between his results and ours would seem to indicate that his variational ansatz is a good one.
 - iv) A similar enhancement of pairing in the odd-parity singlet channel, analogous to our p -wave state, was also noticed for the Hubbard model by Scalettar, Singh and Zhang [42].

Another possibility, however, is that another state in the d -wave sector may cross over the one we have tracked, and become the lowest energy state at large t/J . Such a phenomenon would not be detected by our series analysis.

The formation of a two-hole bound state is not of itself sufficient to prove the existence of either a superconducting condensate, or of “phase separation” between filled and empty sites [1]; but one would certainly presume it to be a necessary precondition for either of these phenomena to occur. Our results indicate that the d -wave binding energy vanishes at around $t/J \simeq 2.5$. The p -wave binding energy may continue a little longer, but it is certainly very weak, and our error bars are not small enough to allow any definite conclusion on this point. Boninsegni and Manousakis [12] and Poilblanc *et al.* [9] found the binding to disappear at around $t/J \simeq 3.7$.

The question of phase separation is still under debate: see the review by Dagotto [1]. At small t/J phase separation is known to occur. Emery, Kivelson and Lin [43] suggested that in fact phase separation occurs at *all* couplings in the neighborhood of half-filling. Subsequently, the majority of studies [1,39] concluded that at intermediate coupling ($0.3 < J/t < 1$) there is a region where binding of pairs occurs, but no phase separation. Poilblanc [44] and Kohno [45] put the phase separation boundary at about $t/J \simeq 1.3$. But Hellberg and Manousakis [39] have recently challenged this scenario, arguing that the criterion of a vanishing inverse compressibility used in previous studies was unreliable. They use a Maxwell construction technique, from which they conclude that indeed phase separation occurs at all couplings in accordance with the original hypothesis of Emery *et al.* [43]. Our results unfortunately have no direct bearing on this debate. To explore these questions one must treat the model away from half-filling, which is not possible using our present series technique, because it cannot handle an unperturbed ground state which is “doped” away from half-filling, and is therefore inhomogeneous.

The presence or absence of a superconducting condensate is also a matter of debate [1]. One recent study [46] found no evidence of d -wave superconducting correlations in the *physical* parameter range $t/J \geq 2$. The simple t - J model is beginning to seem a little doubtful as a theory of the high- T_c superconductors.

There are a number of other significant physical quantities, such as spectral functions, spectral weights, and magnetic susceptibilities which are the subject of ongoing work.

ACKNOWLEDGMENTS

We are grateful to Profs. H.Q. Lin and O. Sushkov for their useful advice, and to Profs. Rajiv R.P. Singh, R. Eder and A.L. Chernyshev for very helpful correspondence. This work forms part of a research project supported by a grant from the Australian Research Council. The computation has been performed on Silicon Graphics Power Challenge and Convex machines. We thank the New South Wales Centre for Parallel Computing for facilities and assistance with the calculations.

REFERENCES

- * e-mail address: C.Hamer@unsw.edu.au
† e-mail address: w.zheng@unsw.edu.au
‡ e-mail address: otja@newt.phys.unsw.edu.au
- [1] E. Dagotto, Rev. Mod. Phys. **66**, 763(1994).
 - [2] E. Dagotto, T.M. Rice, Science **271**, 618(1996); T.M. Rice, Z. Phys. B**103**, 165(1997).
 - [3] L. Yu, Z.B. Su, and Y.M. Li, Chin. J. Phys. **31**, 579(1993).
 - [4] J. Hirsch, Phys. Rev. Lett. **54**, 1317(1985).
 - [5] M.S. Hybertson, E.B. Stechel, M. Schluter and D.R. Jennison, Phys. Rev. B **41**, 11068(1990).
 - [6] F.C. Zhang and T.M. Rice, Phys. Rev. B **37**, 3759(1988).
 - [7] E. Manousakis, Rev. Mod. Phys. **63**, 1(1991).
 - [8] T. Barnes, E. Dagotto, A. Moreo and E.S. Swanson, Phys. Rev. B**40**, 10977(1989); T. Barnes, A.E. Jacobs, M.D. Kovarik and W.G. Macready, Phys. Rev. B **45**, 256(1992).
 - [9] D. Poilblanc, J. Riera and E. Dagotto, Phys. Rev. B **49**, 12318(1994).
 - [10] P.W. Leung and R.J. Gooding, Phys. Rev. B **52**, 15711(1995).
 - [11] T.K. Lee and C.T. Shih, Phys. Rev. B **55**, 5983(1997).
 - [12] M. Boninsegni and E. Manousakis, Phys. Rev. B **47**, 11897(1993).
 - [13] Z.P. Liu and E. Manousakis, Phys. Rev. B **45**, 2425(1992).
 - [14] R. Eder, Phys. Rev. B **45**, 319(1992).
 - [15] M.Yu. Kuchiev and O.P. Sushkov, Phys. Rev. B **52**, 12977(1995).
 - [16] Y.M. Li, N. d'Ambrumenil, L. Yu and Z.B. Su, Phys. Rev. B**53**, 14717(1996).
 - [17] V.I. Belinicher, A.L. Chernyshev and V.A. Shubin, Phys. Rev. B **56**, 3381(1997).
 - [18] B. Shraiman and E. Siggia, Phys. Rev. Lett. **62**, 1564(1989).
 - [19] M. Kuchiev and O. Sushkov, Phys. Rev. B **52**, 12977(1995).
 - [20] H.X. He, C.J. Hamer and J. Oitmaa, J. Phys. A **23**, 1775(1990).
 - [21] J. Oitmaa, C.J. Hamer and W.H. Zheng, Phys. Rev. B **50**, 3877(1994).
 - [22] J. Oitmaa and W.H. Zheng, Phys. Rev. B **54**, 3022(1996).
 - [23] R.R.P. Singh, Phys. Rev. B **39**, 9760(1989); **41**, 4873(1990).
 - [24] M. P. Gelfand, R. R. P. Singh and D. A. Huse, J. Stat. Phys. **59**, 1093 (1990).
 - [25] M. P. Gelfand, Solid State Comm. **98**, 11 (1996).
 - [26] Z.P. Shi and R.R.P. Singh, Phys. Rev. B**52**, 9620(1995); Europhys. Lett. **3**, 219(1995).
 - [27] W.O. Putikka, M.U. Luchini and T.M. Rice, Phys. Rev. Lett. **68**, 538(1992); W.O. Putikka, M.U. Luchini and M. Ogato, Phys. Rev. Lett. **69**, 2288(1992).
 - [28] R.R.P. Singh and R.L. Glenister, Phys. Rev. B**46**, 11871(1992).
 - [29] A.J. Guttmann, in *Phase Transitions and Critical Phenomena*, edited by C. Domb and M.S. Green (Academic, New York, 1989), Vol. 13.
 - [30] R. Eder and K.W. Becker and W.H. Stephan, Z. Phys. B **81**, 33 (1990); R. Eder and K.W. Becker, Z. Phys. B **78**, 219 (1990).
 - [31] G. Martinez and P. Horsch, Phys. Rev. B **44**, 317(1991).
 - [32] N. Bulut, D. Hone and D.J. Scalapino, Phys. Rev. Lett. **62**, 2192(1989).
 - [33] T. Barnes and M.D. Kovarik, Phys. Rev. B **42**, 6159(1990).
 - [34] S. Sachdev, Phys. Rev. B **39**, 12232(1989).
 - [35] A.L. Chernyshev, P.W. Leung and R.J. Gooding, cond-mat/9806018.

- [36] M.A. Baranov and M.Y. Kagan, Z. Phys. B**86**, 237(1992); M.A. Baranov, A.V. Chubukov and M.Y. Kagan, Int. J. Mod. Phys. B**6**, 2411(1992).
- [37] A.V. Chubukov, Phys. Rev. Lett. B**48**, 1097(1993).
- [38] E. Dagotto and J. Riera, Phys. Rev. Lett. **70**, 682(1993); E. Dagotto, J. Riera, Y.C. Chen, A. Moreo, A. Nazarenko, F. Alcaraz and F. Ortolani, Phys. Rev. B**49**, 3548(1994).
- [39] C.S. Hellberg and E. Manousakis, Phys. Rev. Letts. **78**, 4609(1997), and references therein.
- [40] M.Y. Kagan and T.M. Rice, J. Phys. Cond. Mat. **6**, 3771(1994).
- [41] J. Riera and E. Dagotto, Phys. Rev. B**47**, 15346(1993).
- [42] R.T. Scalettar, R.R.P. Singh and S.C. Zhang, Phys. Rev. Lett., **67**, 370(1991).
- [43] V.J. Emery, S.A. Kivelson and H.Q. Lin, Phys. Rev. Lett. **64**, 475(1990); Phys. Rev. B**42**, 6523(1990).
- [44] D. Poiblanc, Phys. Rev. B **52**, 9201(1995).
- [45] M. Kohno, Phys. Rev. B **55**, 1435(1997).
- [46] C.T. Shih, Y.C. Chen, H.Q. Lin and T.K. Lee, cond-mat/9807027.

FIGURES

FIG. 1. (a) The open (full) points represent the up (down) sublattices, respectively. The primitive translation vectors, (e_x, e_y) and $(e_{x'}, e_{y'})$, are shown by the arrows. (b) The reciprocal space of these lattices. The Brillouin zones for (e_x, e_y) and $(e_{x'}, e_{y'})$ are $-\pi/a < k_x, k_y \leq \pi/a$ and $-\pi/(\sqrt{2}a) < k_{x'}, k_{y'} \leq \pi/(\sqrt{2}a)$, respectively, where a is the lattice spacing.

FIG. 2. The extrapolation of the x -series for one-hole energy E^{1h}/J_z for $y = 0.5$ at momentum $\mathbf{k} = (\pi/2, \pi/2)$ and several different r values. Several different integrated differential approximants to the series are shown. The final estimate at $x = 1$ is shown as a cross with error bar.

FIG. 3. Plot of one-hole dispersion Δ/J (where $\Delta \equiv E^{1h}(\mathbf{k}) - E^{1h}(0, 0)$) along the path $\Gamma MX\Gamma$ in the Brillouin zone (see Fig. 1(b)) for the system with coupling ratios $t/J = 1/10, 1/5, 1/3, 1/2, 2/3$ and 1.

FIG. 4. Similar to Fig. 3, but with the hole dispersion curve plotted along the path $\Gamma SM'\Gamma$ in the Brillouin zone.

FIG. 5. The normalized bandwidth $W/t = [E^{1h}(0, 0) - E^{1h}(\pi/2, \pi/2)]/t$ as a function of J/t . The solid square points with error bars connected by a solid line are our estimates from x -series, while the dashed line are our results in Eq.(15) obtained from the two-variable expansions. The crosses are the estimates of Martinez and Horsch [31], the solid circles are the estimates of Liu and Manousakis [13].

FIG. 6. (a) The open (full) points represent the up (down) sublattices, respectively, while the crosses represent the centre points of bonds connecting two adjacent sites. The primitive translation vectors, (e_x, e_y) and $(e_{x'}, e_{y'})$, are shown by the arrows. (b) The reciprocal space of these lattices. The Brillouin zones for (e_x, e_y) and $(e_{x'}, e_{y'})$ are $-\sqrt{2}\pi/a < k_x, k_y \leq \sqrt{2}\pi/a$ and $-\pi/(\sqrt{2}a) < k_{x'}, k_{y'} \leq \pi/(\sqrt{2}a)$, respectively.

FIG. 7. Plot of 2-hole dispersion $E^{2h}(\mathbf{k})/J$ along high-symmetry cuts through the Brillouin zone for the system with coupling ratios $J/t = 10, 5, 3, 2, 3/2$.

FIG. 8. Plot of the estimated binding energy E_b/J for s -, p - and d -wave pair states (marked by s, p and d, respectively) as functions of t/J . The crosses with error bars connected by dashed lines are our estimates from x -series, while the solid lines in the small t/J region are our results in Eq.(20) obtained from the two-variable expansions. The three solid circles with error bars are 8×8 Green's function Monte Carlo results taken from Ref. [12], the five solid triangles are the results of 32-site finite lattice calculations [46,35], while the two open circles are the extrapolation to bulk limit from finite size calculations [35].

FIG. 9. Plot of the one-hole dispersion Δ/J_z (where $\Delta \equiv E^{1h}(\mathbf{k}) - E^{1h}(0,0)$) along the path $\Gamma M X \Gamma$ in the Brillouin zone (see Fig. 1(b)) for the t - J_z model with coupling ratios $t/J_z=5/3, 5/4, 1$ and 0.8 .

FIG. 10. Plot of the one-hole energy at $\mathbf{k} = 0$ for the $t - J_z$ model as a function of $(J_z/t)^{2/3}/[1 + (J_z/t)^{2/3}]$. The solid curves in the large $(J_z/t)^{2/3}/[1 + (J_z/t)^{2/3}]$ region are the integrated differential approximants to the t/J_z series, the points with error bars are estimates from x -series, while the solid curve in the small $(J_z/t)^{2/3}/[1 + (J_z/t)^{2/3}]$ region is the least square fit $E^{1h}/t = -3.60 + 2.9(J_z/t)^{2/3} + J_z/t$ to the results in the interval $0.2 \leq J_z/t \leq 1$.

FIG. 11. Plot of the 2-hole dispersion $E^{2h}(\mathbf{k})/J_z$ along high-symmetry cuts through the Brillouin zone for the t - J_z model with coupling ratios $t/J_z = 0.2, 0.4, 0.6, 0.8$ and 1 .

FIG. 12. Plot of the binding energy E_b/J as a function of t/J_z for the t - J_z model. The solid lines are the different integrated differential approximants to the expansion in t/J_z , while the points with error bars connected by dashed lines are the estimates from the expansion in x . The solid points are the results of a finite size calculations [41].

TABLES

TABLE I. Series coefficients for the one-hole energy $E^{1h}/J_z = \sum_k c_k x^k$ for $y = 0.5$ at $\mathbf{k} = (\pi/2, \pi/2)$ for the t - J model. Nonzero coefficients c_i up to order $k = 11$ for $r = 0, 1, 2, 4, 8$ are listed.

k	$r = 0$	$r = 1$	$r = 2$	$r = 4$	$r = 8$
0	2.000000000	2.500000000	3.000000000	4.000000000	6.000000000
1	0.000000000	$-5.000000000 \times 10^{-1}$	-1.000000000	-2.000000000	-4.000000000
2	$-5.333333333 \times 10^{-1}$	$-2.666666667 \times 10^{-1}$	$-1.758241758 \times 10^{-1}$	$-1.038961039 \times 10^{-1}$	$-5.689900427 \times 10^{-2}$
3	$-2.666666667 \times 10^{-1}$	$-2.251851852 \times 10^{-1}$	$-1.647144065 \times 10^{-1}$	$-1.027716872 \times 10^{-1}$	$-5.729559761 \times 10^{-2}$
4	$2.062354497 \times 10^{-1}$	$-8.432815051 \times 10^{-2}$	$-1.116301281 \times 10^{-1}$	$-8.974496745 \times 10^{-2}$	$-5.525294748 \times 10^{-2}$
5	$2.121710758 \times 10^{-1}$	$1.942107294 \times 10^{-2}$	$-5.439972676 \times 10^{-2}$	$-7.119994116 \times 10^{-2}$	$-5.149488552 \times 10^{-2}$
6	$-2.058364193 \times 10^{-2}$	$4.770714647 \times 10^{-2}$	$-1.307093131 \times 10^{-2}$	$-5.177543994 \times 10^{-2}$	$-4.663864987 \times 10^{-2}$
7	$-2.275638025 \times 10^{-1}$	$2.527038112 \times 10^{-2}$	$7.461856693 \times 10^{-3}$	$-3.440622079 \times 10^{-2}$	$-4.119274206 \times 10^{-2}$
8	$-9.889853918 \times 10^{-2}$	$-7.079155979 \times 10^{-3}$	$1.149881952 \times 10^{-2}$	$-2.058064339 \times 10^{-2}$	$-3.556056761 \times 10^{-2}$
9	$1.839605467 \times 10^{-1}$	$-2.298423843 \times 10^{-2}$	$6.622730013 \times 10^{-3}$	$-1.069884345 \times 10^{-2}$	$-3.004823602 \times 10^{-2}$
10	$2.267402233 \times 10^{-1}$	$-1.850514883 \times 10^{-2}$	$-3.889599620 \times 10^{-4}$	$-4.444287027 \times 10^{-3}$	$-2.487508963 \times 10^{-2}$
11	$-9.850744312 \times 10^{-2}$	$-4.463638360 \times 10^{-3}$	$-5.435829342 \times 10^{-3}$	$-1.112182682 \times 10^{-3}$	$-2.018574494 \times 10^{-2}$

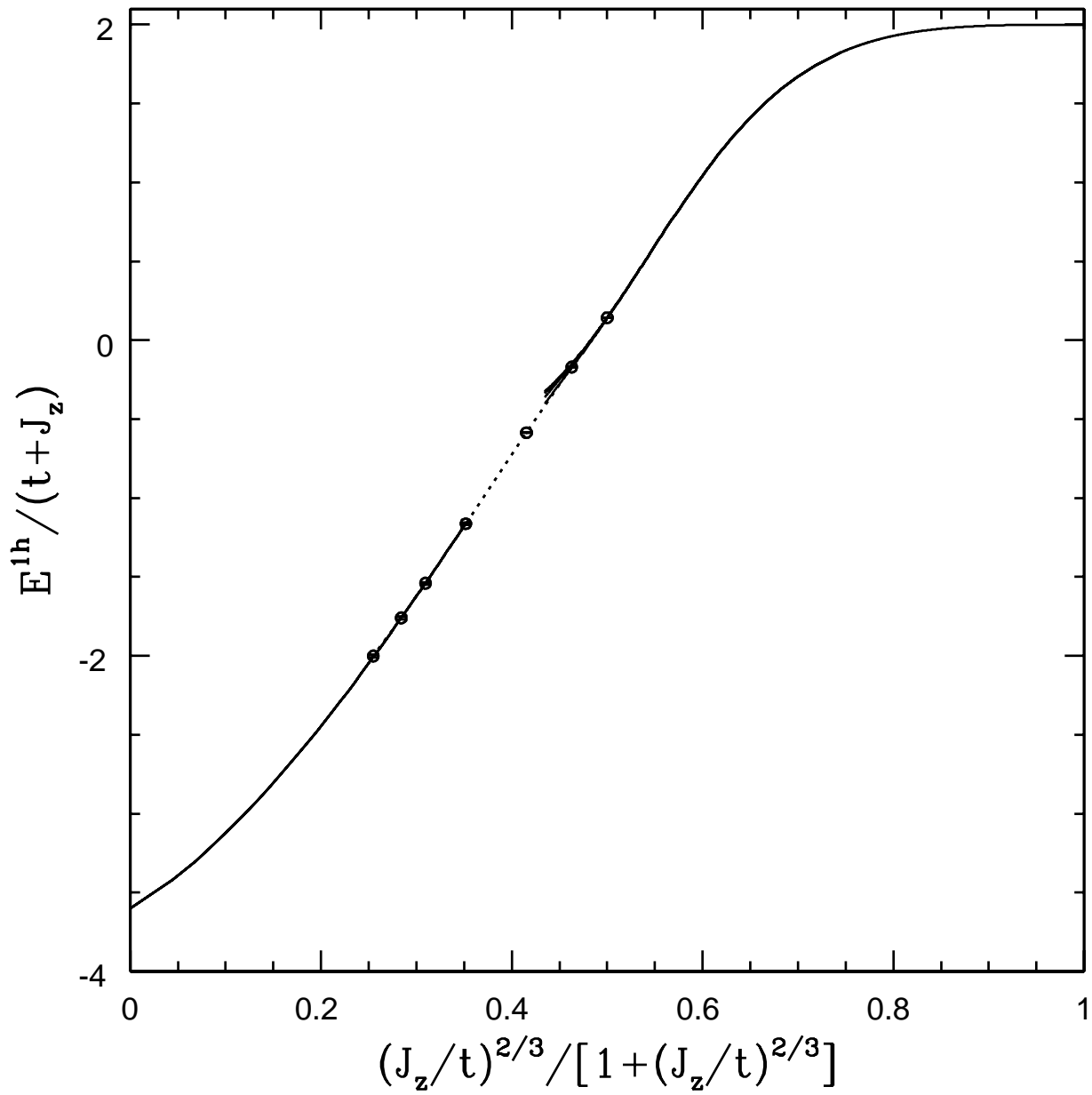
TABLE II. Series coefficients for the one-hole and two-hole energy $E(k_x, k_y)/J_z = \sum_{k,n,m} a_{k,n,m} x^k [\cos(nk_x A) \cos(mk_y A) + \cos(mk_x A) \cos(nk_y A)]/2$ of the t - J model, where $A = a$ for the one-hole case and $A = a/\sqrt{2}$ for the two-hole case. Nonzero coefficients $a_{k,n,m}$ up to order $k = 11$ for $y = 0.5$ and $r = 0$ are listed.

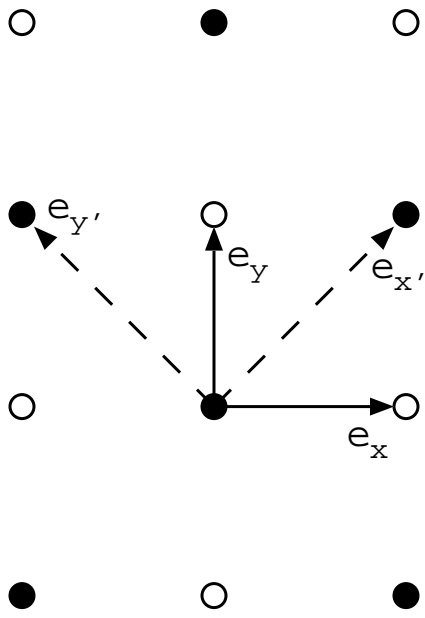
(k,n,m)	$a_{k,n,m}$	(k,n,m)	$a_{k,n,m}$	(k,n,m)	$a_{k,n,m}$	(k,n,m)	$a_{k,n,m}$
one hole energy $E^{1h}(k_x, k_y)/J_z$							
(0, 0, 0)	2.000000000	(8, 2, 0)	-8.693161815 $\times 10^{-2}$	(5, 1, 1)	-3.650599647 $\times 10^{-1}$	(11, 5, 1)	-2.756493796 $\times 10^{-2}$
(2, 0, 0)	-5.333333333 $\times 10^{-1}$	(9, 2, 0)	2.176985203 $\times 10^{-1}$	(6, 1, 1)	2.714260859 $\times 10^{-1}$	(6, 2, 2)	7.130158730 $\times 10^{-2}$
(4, 0, 0)	1.529021164 $\times 10^{-1}$	(10, 2, 0)	-1.017391598 $\times 10^{-2}$	(7, 1, 1)	2.890627842 $\times 10^{-1}$	(7, 2, 2)	-6.731669606 $\times 10^{-2}$
(5, 0, 0)	9.481481481 $\times 10^{-2}$	(11, 2, 0)	-3.628184110 $\times 10^{-1}$	(8, 1, 1)	-2.000742064 $\times 10^{-1}$	(8, 2, 2)	-1.075223788 $\times 10^{-1}$
(6, 0, 0)	-1.772367448 $\times 10^{-2}$	(6, 4, 0)	1.188359788 $\times 10^{-2}$	(9, 1, 1)	-1.603987396 $\times 10^{-1}$	(9, 2, 2)	1.539341160 $\times 10^{-1}$
(7, 0, 0)	-1.684678469 $\times 10^{-1}$	(7, 4, 0)	-4.980599647 $\times 10^{-3}$	(10, 1, 1)	-1.153947213 $\times 10^{-1}$	(10, 2, 2)	9.103499935 $\times 10^{-2}$
(8, 0, 0)	-6.427987242 $\times 10^{-2}$	(8, 4, 0)	-1.402790612 $\times 10^{-2}$	(11, 1, 1)	1.409738327 $\times 10^{-1}$	(11, 2, 2)	-2.080643863 $\times 10^{-1}$
(9, 0, 0)	2.538548842 $\times 10^{-1}$	(9, 4, 0)	2.637981607 $\times 10^{-2}$	(6, 3, 1)	9.506878307 $\times 10^{-2}$	(9, 4, 2)	3.146104767 $\times 10^{-2}$
(10, 0, 0)	1.029816377 $\times 10^{-1}$	(10, 4, 0)	-1.865761552 $\times 10^{-2}$	(7, 3, 1)	-7.727789536 $\times 10^{-2}$	(10, 4, 2)	-4.054217598 $\times 10^{-2}$
(11, 0, 0)	-2.786820323 $\times 10^{-1}$	(11, 4, 0)	-4.652610741 $\times 10^{-2}$	(8, 3, 1)	-1.457528700 $\times 10^{-1}$	(11, 4, 2)	-7.000652266 $\times 10^{-2}$
(3, 2, 0)	2.666666667 $\times 10^{-1}$	(9, 6, 0)	1.048701589 $\times 10^{-3}$	(9, 3, 1)	1.806575878 $\times 10^{-1}$	(9, 3, 3)	2.097403178 $\times 10^{-2}$
(4, 2, 0)	-5.333333333 $\times 10^{-2}$	(10, 6, 0)	-6.651097800 $\times 10^{-4}$	(10, 3, 1)	8.928712117 $\times 10^{-2}$	(10, 3, 3)	-2.874385753 $\times 10^{-2}$
(5, 2, 0)	-1.173562610 $\times 10^{-1}$	(11, 6, 0)	-1.940149264 $\times 10^{-3}$	(11, 3, 1)	-2.245856051 $\times 10^{-1}$	(11, 3, 3)	-4.632188322 $\times 10^{-2}$
(6, 2, 0)	8.604515263 $\times 10^{-2}$	(3, 1, 1)	5.333333333 $\times 10^{-1}$	(9, 5, 1)	1.258441907 $\times 10^{-2}$		
(7, 2, 0)	-1.320134011 $\times 10^{-2}$	(4, 1, 1)	-2.962962963 $\times 10^{-1}$	(10, 5, 1)	-1.312853800 $\times 10^{-2}$		
two-hole energy $E^{2h}(k_x, k_y)/J_z$							
(0, 0, 0)	3.500000000	(6, 3, 3)	1.457965902 $\times 10^{-3}$	(6, 3, 2)	5.831863610 $\times 10^{-3}$	(9, 4, 2)	-7.128118497 $\times 10^{-4}$
(2, 0, 0)	-7.333333333 $\times 10^{-1}$	(8, 3, 3)	-8.399019298 $\times 10^{-3}$	(7, 3, 2)	-4.705118313 $\times 10^{-3}$	(10, 4, 2)	-6.158730192 $\times 10^{-2}$
(4, 0, 0)	1.945310847 $\times 10^{-1}$	(9, 3, 3)	2.106020257 $\times 10^{-2}$	(8, 3, 2)	-5.937350737 $\times 10^{-2}$	(11, 4, 2)	6.702194733 $\times 10^{-2}$
(5, 0, 0)	1.570370370 $\times 10^{-1}$	(10, 3, 3)	5.953632826 $\times 10^{-3}$	(9, 3, 2)	3.295758313 $\times 10^{-2}$	(10, 5, 2)	2.643901061 $\times 10^{-4}$
(6, 0, 0)	-1.814429222 $\times 10^{-1}$	(11, 3, 3)	4.246104998 $\times 10^{-3}$	(10, 3, 2)	1.653086795 $\times 10^{-2}$	(11, 5, 3)	-8.754870105 $\times 10^{-5}$
(7, 0, 0)	3.336368382 $\times 10^{-2}$	(8, 4, 4)	1.843920010 $\times 10^{-4}$	(11, 3, 2)	-1.386696140 $\times 10^{-2}$	(6, 3, 0)	5.831863610 $\times 10^{-3}$
(8, 0, 0)	-1.977570791 $\times 10^{-1}$	(10, 4, 4)	-3.073373856 $\times 10^{-3}$	(8, 4, 3)	7.375680039 $\times 10^{-4}$	(7, 3, 0)	-1.162496326 $\times 10^{-3}$
(9, 0, 0)	-1.214962788 $\times 10^{-1}$	(11, 4, 4)	4.127194476 $\times 10^{-4}$	(9, 4, 3)	-5.394036567 $\times 10^{-4}$	(8, 3, 0)	-1.040888381 $\times 10^{-1}$
(10, 0, 0)	1.897994391 $\times 10^{-1}$	(10, 5, 5)	2.643901061 $\times 10^{-5}$	(10, 4, 3)	-2.344210680 $\times 10^{-2}$	(9, 3, 0)	8.179624689 $\times 10^{-2}$
(11, 0, 0)	7.710636344 $\times 10^{-1}$	(2, 1, 0)	6.666666667 $\times 10^{-1}$	(11, 4, 3)	3.300423401 $\times 10^{-2}$	(10, 3, 0)	1.171660236 $\times 10^{-1}$
(2, 1, 1)	3.333333333 $\times 10^{-1}$	(3, 1, 0)	3.333333333 $\times 10^{-1}$	(10, 5, 4)	1.057560424 $\times 10^{-4}$	(11, 3, 0)	1.531781787 $\times 10^{-2}$
(3, 1, 1)	-3.333333333 $\times 10^{-1}$	(4, 1, 0)	-2.673809524 $\times 10^{-1}$	(11, 5, 4)	-7.959003190 $\times 10^{-5}$	(8, 4, 1)	2.212704012 $\times 10^{-3}$
(4, 1, 1)	-1.192857143 $\times 10^{-1}$	(5, 1, 0)	-4.024977954 $\times 10^{-1}$	(4, 2, 0)	2.962962963 $\times 10^{-2}$	(9, 4, 1)	-8.862200427 $\times 10^{-4}$
(5, 1, 1)	2.904905203 $\times 10^{-1}$	(6, 1, 0)	-1.302727805 $\times 10^{-1}$	(5, 2, 0)	-2.629629630 $\times 10^{-2}$	(10, 4, 1)	-9.978608234 $\times 10^{-2}$
(6, 1, 1)	5.329329186 $\times 10^{-1}$	(7, 1, 0)	3.499536691 $\times 10^{-1}$	(6, 2, 0)	-2.375711537 $\times 10^{-1}$	(11, 4, 1)	1.153622881 $\times 10^{-1}$
(7, 1, 1)	-6.271803816 $\times 10^{-1}$	(8, 1, 0)	4.079418136 $\times 10^{-1}$	(7, 2, 0)	2.330090787 $\times 10^{-1}$	(10, 5, 2)	4.230241698 $\times 10^{-4}$
(8, 1, 1)	-7.522337850 $\times 10^{-1}$	(9, 1, 0)	5.301735104 $\times 10^{-2}$	(8, 2, 0)	3.039557383 $\times 10^{-1}$	(11, 5, 2)	-1.750974021 $\times 10^{-4}$
(9, 1, 1)	5.347837206 $\times 10^{-1}$	(10, 1, 0)	-1.026434348	(9, 2, 0)	-3.529882617 $\times 10^{-1}$	(8, 4, 0)	1.106352006 $\times 10^{-3}$
(10, 1, 1)	1.146091910	(11, 1, 0)	-7.412817539 $\times 10^{-1}$	(10, 2, 0)	-6.813379022 $\times 10^{-1}$	(9, 4, 0)	-7.128118497 $\times 10^{-4}$
(11, 1, 1)	-4.863394606 $\times 10^{-1}$	(4, 2, 1)	5.925925926 $\times 10^{-2}$	(11, 2, 0)	9.790814131 $\times 10^{-1}$	(10, 4, 0)	-5.538838348 $\times 10^{-2}$
(4, 2, 2)	1.481481481 $\times 10^{-2}$	(5, 2, 1)	-2.629629630 $\times 10^{-2}$	(6, 3, 1)	8.747795414 $\times 10^{-3}$	(11, 4, 0)	8.043954590 $\times 10^{-2}$
(6, 2, 2)	-5.533170820 $\times 10^{-2}$	(6, 2, 1)	-8.610412317 $\times 10^{-2}$	(7, 3, 1)	-5.867614638 $\times 10^{-3}$	(10, 5, 1)	5.287802122 $\times 10^{-4}$
(7, 2, 2)	1.147526740 $\times 10^{-2}$	(7, 2, 1)	5.769980192 $\times 10^{-2}$	(8, 3, 1)	-1.459267389 $\times 10^{-1}$	(11, 5, 1)	-2.626461032 $\times 10^{-4}$
(8, 2, 2)	3.484612337 $\times 10^{-2}$	(8, 2, 1)	2.118965896 $\times 10^{-1}$	(9, 3, 1)	1.611775400 $\times 10^{-1}$	(10, 5, 0)	3.172681273 $\times 10^{-4}$
(9, 2, 2)	-8.489781072 $\times 10^{-2}$	(9, 2, 1)	-9.184491129 $\times 10^{-2}$	(10, 3, 1)	1.623787831 $\times 10^{-1}$	(11, 5, 0)	-9.550737020 $\times 10^{-5}$
(10, 2, 2)	-8.365174384 $\times 10^{-2}$	(10, 2, 1)	-3.638022235 $\times 10^{-1}$	(11, 3, 1)	-3.687197934 $\times 10^{-1}$		
(11, 2, 2)	3.945274143 $\times 10^{-1}$	(11, 2, 1)	-5.611998341 $\times 10^{-3}$	(8, 4, 2)	1.475136008 $\times 10^{-3}$		

TABLE III. Series coefficients for the one-hole and two-hole energy $E(k_x, k_y)/J_z = \sum_{k,n,m} a_{k,n,m} (t/J_z)^k [\cos(nk_x A) \cos(mk_y A) + \cos(mk_x A) \cos(nk_y A)]/2$ for the Hamiltonian in Eq. (21) of the t - J_z model, where $A = a$ for the one-hole case and $A = a/\sqrt{2}$ for the two-hole case. Nonzero coefficients $a_{k,n,m}$ up to order $k = 20$ for one-hole case or $k = 18$ for two-hole case are listed.

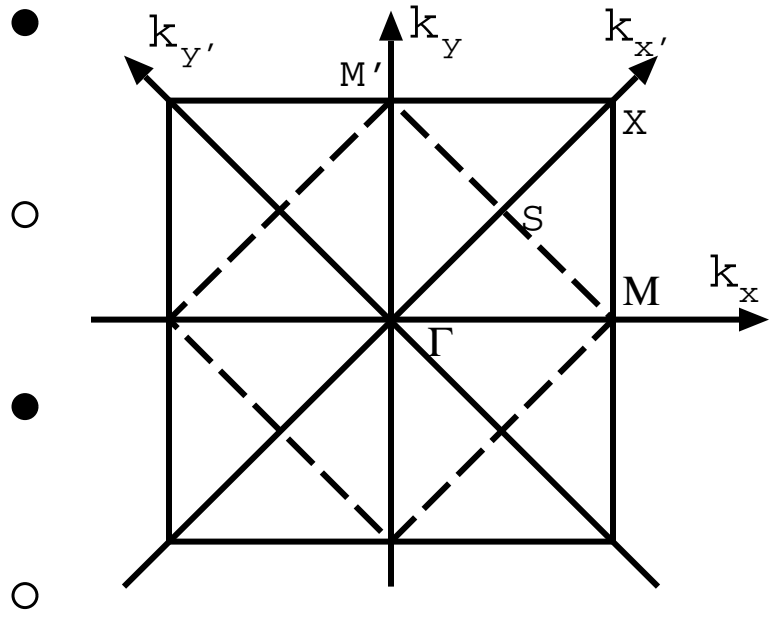
(k,n,m)	$a_{k,n,m}$	(k,n,m)	$a_{k,n,m}$	(k,n,m)	$a_{k,n,m}$	(k,n,m)	$a_{k,n,m}$
one hole energy $E^{1h}(k_x, k_y)/J_z$							
(0, 0, 0)	2.000000000	(20, 0, 0)	3.269830958×10^4	(8, 1, 1)	1.107677837	(20, 3, 1)	1.363566623
(2, 0, 0)	-2.666666667	(10, 2, 0)	$-9.187011686 \times 10^{-3}$	(10, 1, 1)	-5.258263841	(12, 2, 2)	$2.213826787 \times 10^{-2}$
(4, 0, 0)	2.607407407	(12, 2, 0)	$1.237459977 \times 10^{-1}$	(12, 1, 1)	2.361854957×10^1	(14, 2, 2)	$-2.801396443 \times 10^{-1}$
(6, 0, 0)	-5.667818930	(14, 2, 0)	-1.042288265	(14, 1, 1)	-1.041949744×10^2	(16, 2, 2)	2.293697931
(8, 0, 0)	1.579276071×10^1	(16, 2, 0)	7.139692772	(16, 1, 1)	4.570753372×10^2	(18, 2, 2)	-1.550982309×10^1
(10, 0, 0)	-4.977461910×10^1	(18, 2, 0)	-4.367374242×10^1	(18, 1, 1)	-2.003192131×10^3	(20, 2, 2)	9.435217647×10^1
(12, 0, 0)	1.689229038×10^2	(20, 2, 0)	2.492266705×10^2	(20, 1, 1)	8.787977137×10^3	(20, 4, 2)	$4.053738087 \times 10^{-5}$
(14, 0, 0)	-6.023423934×10^2	(18, 4, 0)	$-1.275445883 \times 10^{-6}$	(14, 3, 1)	$-1.112602736 \times 10^{-4}$	(18, 3, 3)	$-4.160122546 \times 10^{-3}$
(16, 0, 0)	2.225264150×10^3	(20, 4, 0)	$1.432818794 \times 10^{-4}$	(16, 3, 1)	$6.891013162 \times 10^{-3}$	(20, 3, 3)	$8.089745849 \times 10^{-2}$
(18, 0, 0)	-8.447437043×10^3	(6, 1, 1)	$-1.896296296 \times 10^{-1}$	(18, 3, 1)	$-1.208165780 \times 10^{-1}$		
two-hole energy $E^{2h}(k_x, k_y)/J_z$							
(0, 0, 0)	3.500000000	(2, 1, 0)	2.666666667	(10, 3, 1)	-3.833568660	(10, 4, 0)	$-4.187749256 \times 10^{-1}$
(2, 0, 0)	-4.000000000	(4, 1, 0)	-2.607407407	(12, 3, 1)	3.749428458×10^1	(12, 4, 0)	-4.625682644
(4, 0, 0)	2.311111111	(6, 1, 0)	$-9.124044680 \times 10^{-1}$	(14, 3, 1)	-1.763568623×10^2	(14, 4, 0)	3.879009243×10^1
(6, 0, 0)	$-3.578130511 \times 10^{-1}$	(8, 1, 0)	2.709462265×10^1	(16, 3, 1)	5.362296757×10^2	(16, 4, 0)	-1.755530196×10^2
(8, 0, 0)	-1.447791909×10^1	(10, 1, 0)	-1.454354060×10^2	(18, 3, 1)	-4.338040480×10^2	(18, 4, 0)	5.141129944×10^2
(10, 0, 0)	8.449051521×10^1	(12, 1, 0)	4.973154521×10^2	(8, 4, 2)	$3.776348180 \times 10^{-1}$	(10, 5, 1)	$3.414709373 \times 10^{-1}$
(12, 0, 0)	-3.205718341×10^2	(14, 1, 0)	-8.044807264×10^2	(10, 4, 2)	$-7.694903208 \times 10^{-1}$	(12, 5, 1)	$-6.844512414 \times 10^{-1}$
(14, 0, 0)	7.683946158×10^2	(16, 1, 0)	-3.592648436×10^3	(12, 4, 2)	-3.834200865	(14, 5, 1)	-1.368955321×10^1
(16, 0, 0)	1.864995221×10^2	(18, 1, 0)	4.011882196×10^4	(14, 4, 2)	4.301073460×10^1	(16, 5, 1)	1.169642314×10^2
(18, 0, 0)	-1.447204343×10^4	(4, 2, 1)	$9.481481481 \times 10^{-1}$	(16, 4, 2)	-2.363456039×10^2	(18, 5, 1)	-5.467419040×10^2
(2, 1, 1)	1.333333333	(6, 2, 1)	-2.072004703	(18, 4, 2)	9.094821992×10^2	(12, 6, 2)	$5.024245295 \times 10^{-1}$
(4, 1, 1)	-1.362962963	(8, 2, 1)	1.071796284	(10, 5, 3)	$2.707354687 \times 10^{-1}$	(14, 6, 2)	$-5.607740036 \times 10^{-1}$
(6, 1, 1)	3.117601411	(10, 2, 1)	1.934131152×10^1	(12, 5, 3)	$-6.099856791 \times 10^{-1}$	(16, 6, 2)	-1.688448287×10^1
(8, 1, 1)	-1.157205899×10^1	(12, 2, 1)	-1.610227509×10^2	(14, 5, 3)	-3.591949866	(18, 6, 2)	1.530376091×10^2
(10, 1, 1)	3.724437583×10^1	(14, 2, 1)	9.100666397×10^2	(16, 5, 3)	4.680082984×10^1	(14, 7, 3)	$4.576926174 \times 10^{-1}$
(12, 1, 1)	-4.436033620×10^1	(16, 2, 1)	-4.053430224×10^3	(18, 5, 3)	-2.944841481×10^2	(16, 7, 3)	$-4.694339733 \times 10^{-1}$
(14, 1, 1)	-5.334708723×10^2	(18, 2, 1)	1.279544679×10^4	(12, 6, 4)	$2.009698118 \times 10^{-1}$	(18, 7, 3)	-1.886986003×10^1
(16, 1, 1)	5.421019234×10^3	(6, 3, 2)	$3.732392710 \times 10^{-1}$	(14, 6, 4)	$-4.925030503 \times 10^{-1}$	(16, 8, 4)	$4.117367040 \times 10^{-1}$
(18, 1, 1)	-3.093983511×10^4	(8, 3, 2)	$-7.739781828 \times 10^{-1}$	(16, 6, 4)	-3.212472559	(18, 8, 4)	$-4.052076547 \times 10^{-1}$
(4, 2, 2)	$2.370370370 \times 10^{-1}$	(10, 3, 2)	-1.053007756	(18, 6, 4)	4.903204193×10^1	(18, 9, 5)	$3.670192948 \times 10^{-1}$
(6, 2, 2)	$-5.237389771 \times 10^{-1}$	(12, 3, 2)	1.967483048×10^1	(14, 7, 5)	$1.525642058 \times 10^{-1}$	(10, 5, 0)	$3.248825624 \times 10^{-1}$
(8, 2, 2)	1.010441376	(14, 3, 2)	-1.305817944×10^2	(16, 7, 5)	$-4.034853659 \times 10^{-1}$	(12, 5, 0)	$-6.899424873 \times 10^{-1}$
(10, 2, 2)	-1.494008026	(16, 3, 2)	6.744405152×10^2	(18, 7, 5)	-2.770916581	(14, 5, 0)	-6.463536863
(12, 2, 2)	$1.846909265 \times 10^{-1}$	(18, 3, 2)	-2.972249754×10^3	(16, 8, 6)	$1.176390583 \times 10^{-1}$	(16, 5, 0)	6.567477615×10^1
(14, 2, 2)	1.06276508×10^1	(8, 4, 3)	$1.888174090 \times 10^{-1}$	(18, 8, 6)	$-3.342928209 \times 10^{-1}$	(18, 5, 0)	-3.388841937×10^2
(16, 2, 2)	-1.111625374×10^2	(10, 4, 3)	$-2.886375899 \times 10^{-1}$	(18, 9, 7)	$9.175482371 \times 10^{-2}$	(12, 6, 1)	$6.698993726 \times 10^{-1}$
(18, 2, 2)	1.249271047×10^3	(12, 4, 3)	-1.577708121	(6, 3, 0)	$3.732392710 \times 10^{-1}$	(14, 6, 1)	-1.079421253
(6, 3, 3)	$9.330981775 \times 10^{-2}$	(14, 4, 3)	1.855760450×10^1	(8, 3, 0)	$-9.806190570 \times 10^{-1}$	(16, 6, 1)	-2.116718725×10^1
(8, 3, 3)	$-2.869718840 \times 10^{-1}$	(16, 4, 3)	-1.206715261×10^2	(10, 3, 0)	$-7.606578761 \times 10^{-1}$	(18, 6, 1)	2.016971553×10^2
(10, 3, 3)	$7.302649849 \times 10^{-1}$	(18, 4, 3)	6.228213110×10^2	(12, 3, 0)	1.900360917×10^1	(14, 7, 2)	$6.538465963 \times 10^{-1}$
(12, 3, 3)	$6.474454323 \times 10^{-2}$	(10, 5, 4)	$1.082941875 \times 10^{-1}$	(14, 3, 0)	-1.096944607×10^2	(16, 7, 2)	$-6.381513372 \times 10^{-1}$
(14, 3, 3)	-1.507976852×10^1	(12, 5, 4)	$-7.182655253 \times 10^{-2}$	(16, 3, 0)	4.525126033×10^2	(18, 7, 2)	-2.878600133×10^1
(16, 3, 3)	1.112739551×10^2	(14, 5, 4)	-1.662709009	(18, 3, 0)	-1.604127694×10^3	(16, 8, 3)	$6.176050560 \times 10^{-1}$
(18, 3, 3)	-5.501017323×10^2	(16, 5, 4)	1.713732791×10^1	(8, 4, 1)	$5.664522270 \times 10^{-1}$	(18, 8, 3)	$-1.660697208 \times 10^{-1}$
(8, 4, 4)	$4.720435225 \times 10^{-2}$	(18, 5, 4)	-1.134996640×10^2	(10, 4, 1)	-1.358637239	(18, 9, 4)	$5.709189031 \times 10^{-1}$
(10, 4, 4)	$-1.753576976 \times 10^{-1}$	(12, 6, 5)	$6.698993726 \times 10^{-2}$	(12, 4, 1)	-5.476288758	(12, 6, 0)	$3.349496863 \times 10^{-1}$
(12, 4, 4)	$5.665451332 \times 10^{-1}$	(14, 6, 5)	$2.348849413 \times 10^{-2}$	(14, 4, 1)	6.555818772×10^1	(14, 6, 0)	$-2.248529752 \times 10^{-1}$
(14, 4, 4)	$7.031489323 \times 10^{-1}$	(16, 6, 5)	-1.498021733	(16, 4, 1)	-3.561148091×10^2	(16, 6, 0)	-1.304144759×10^1
(16, 4, 4)	-2.234394856×10^1	(18, 6, 5)	1.514875202×10^1	(18, 4, 1)	1.327749407×10^3	(18, 6, 0)	1.069591051×10^2
(18, 4, 4)	1.696295810×10^2	(14, 7, 6)	$4.358977309 \times 10^{-2}$	(10, 5, 2)	$4.331767498 \times 10^{-1}$	(14, 7, 1)	$7.628210290 \times 10^{-1}$
(10, 5, 5)	$2.707354687 \times 10^{-2}$	(16, 7, 6)	$6.397044909 \times 10^{-2}$	(12, 5, 2)	$-8.287589771 \times 10^{-1}$	(16, 7, 1)	$-1.648715187 \times 10^{-1}$
(12, 5, 5)	$-1.145505796 \times 10^{-1}$	(18, 7, 6)	-1.267992012	(14, 5, 2)	-8.117281873	(18, 7, 1)	-3.918669310×10^1
(14, 5, 5)	$4.544498080 \times 10^{-1}$	(16, 8, 7)	$2.940976457 \times 10^{-2}$	(16, 5, 2)	8.399862105×10^1	(16, 8, 2)	$8.234734079 \times 10^{-1}$
(16, 5, 5)	1.078497914	(18, 8, 7)	$7.770975088 \times 10^{-2}$	(18, 5, 2)	-4.609565870×10^2	(18, 8, 2)	$1.073653528 \times 10^{-1}$
(18, 5, 5)	-2.724985485×10^1	(18, 9, 8)	$2.038996082 \times 10^{-2}$	(12, 6, 3)	$3.349496863 \times 10^{-1}$	(18, 9, 3)	$6.563783546 \times 10^{-1}$
(12, 6, 6)	$1.674748432 \times 10^{-2}$	(4, 2, 0)	$4.740740741 \times 10^{-1}$	(14, 6, 3)	$-4.223690648 \times 10^{-1}$	(14, 7, 0)	$4.358977309 \times 10^{-1}$
(14, 6, 6)	$-7.829101098 \times 10^{-2}$	(6, 2, 0)	$-6.512874780 \times 10^{-1}$	(16, 6, 3)	-9.671323639	(16, 7, 0)	$-4.703472705 \times 10^{-1}$
(16, 6, 6)	$3.741008913 \times 10^{-1}$	(8, 2, 0)	-1.556811959	(18, 6, 3)	9.548744493×10^1	(18, 7, 0)	-1.979896930×10^1
(18, 6, 6)	1.267008305	(10, 2, 0)	1.207544510×10^1	(14, 7, 4)	$2.615386385 \times 10^{-1}$	(16, 8, 1)	1.029341760

(14, 7, 7)	$1.089744327 \times 10^{-2}$	(12, 2, 0)	-3.196277031×10^1	(16, 7, 4)	$-1.332433821 \times 10^{-1}$	(18, 8, 1)	$-4.479185205 \times 10^{-1}$
(16, 7, 7)	$-5.528545914 \times 10^{-2}$	(14, 2, 0)	-5.271684834×10^1	(18, 7, 4)	-1.033273379×10^1	(18, 9, 2)	1.141837806
(18, 7, 7)	$3.138641071 \times 10^{-1}$	(16, 2, 0)	1.018254901×10^3	(16, 8, 5)	$2.058683520 \times 10^{-1}$	(16, 8, 0)	$5.146708800 \times 10^{-1}$
(16, 8, 8)	$7.352441142 \times 10^{-3}$	(18, 2, 0)	-5.459613629×10^3	(18, 8, 5)	$6.203359335 \times 10^{-2}$	(18, 8, 0)	$2.583076501 \times 10^{-1}$
(18, 8, 8)	$-4.001373177 \times 10^{-2}$	(6, 3, 1)	$5.598589065 \times 10^{-1}$	(18, 9, 6)	$1.631196866 \times 10^{-1}$	(18, 9, 1)	1.284567532
(18, 9, 9)	$5.097490206 \times 10^{-3}$	(8, 3, 1)	$-9.918360628 \times 10^{-1}$	(8, 4, 0)	$2.832261135 \times 10^{-1}$	(18, 9, 0)	$7.136486288 \times 10^{-1}$

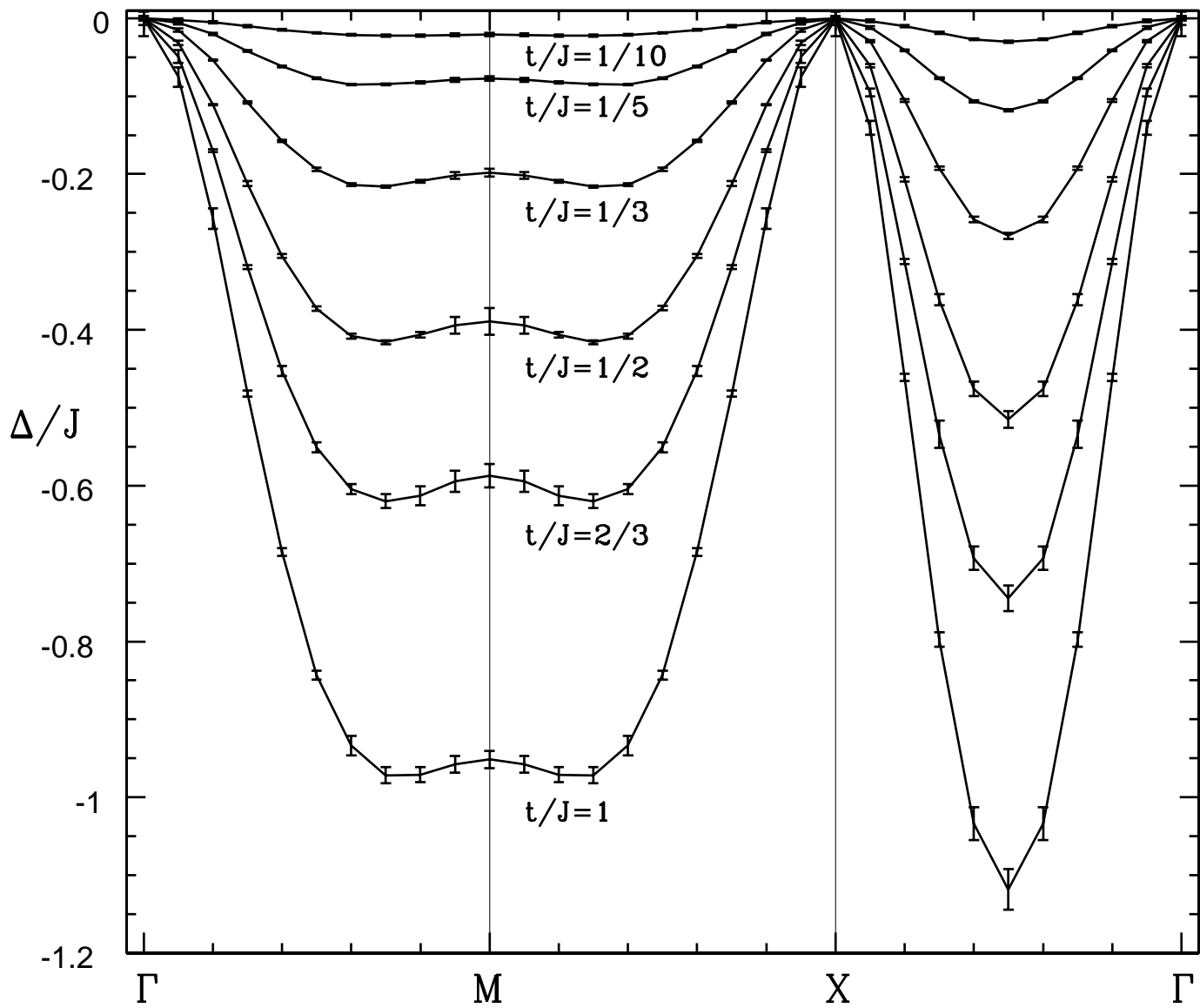


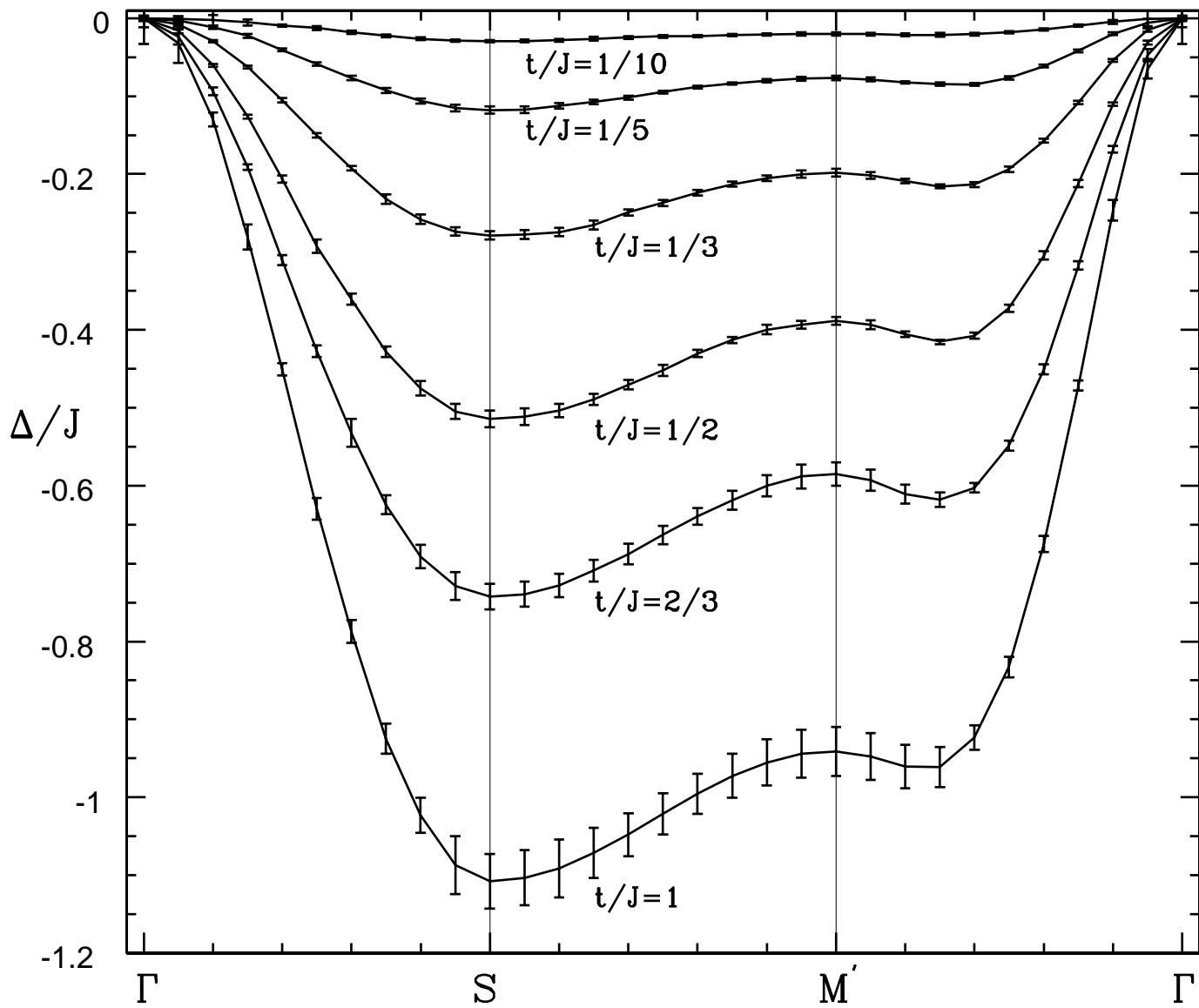


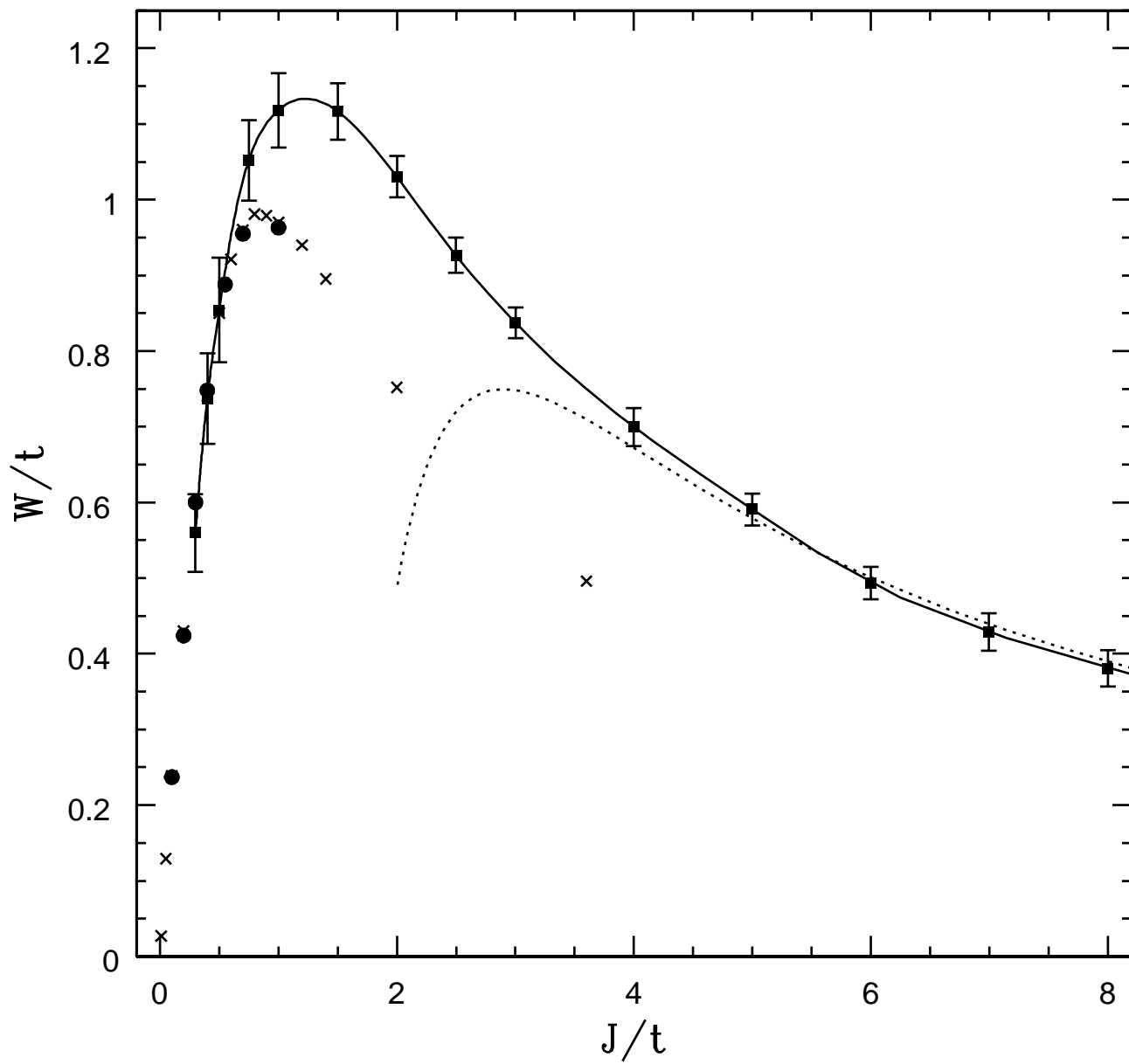
(a)

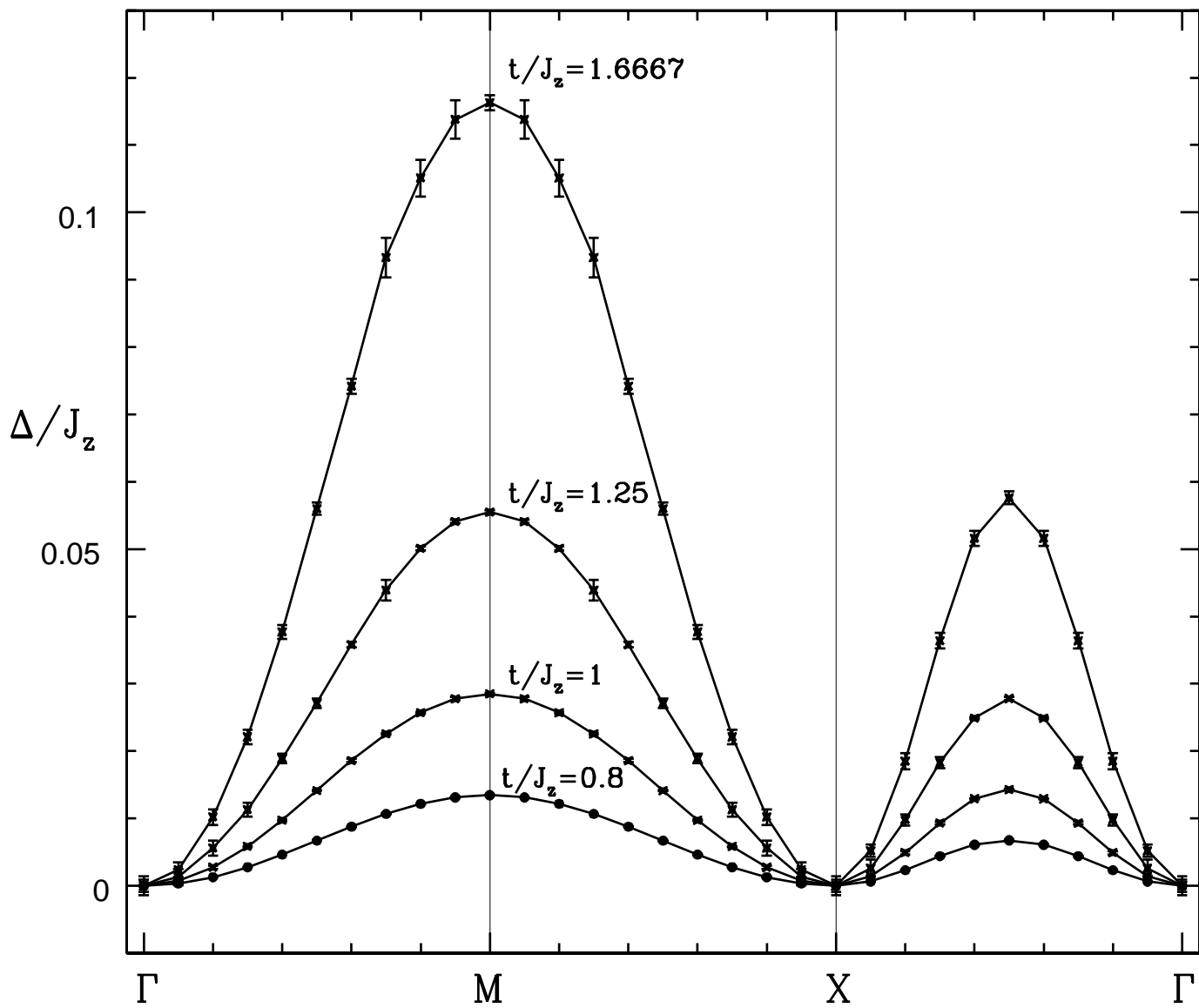


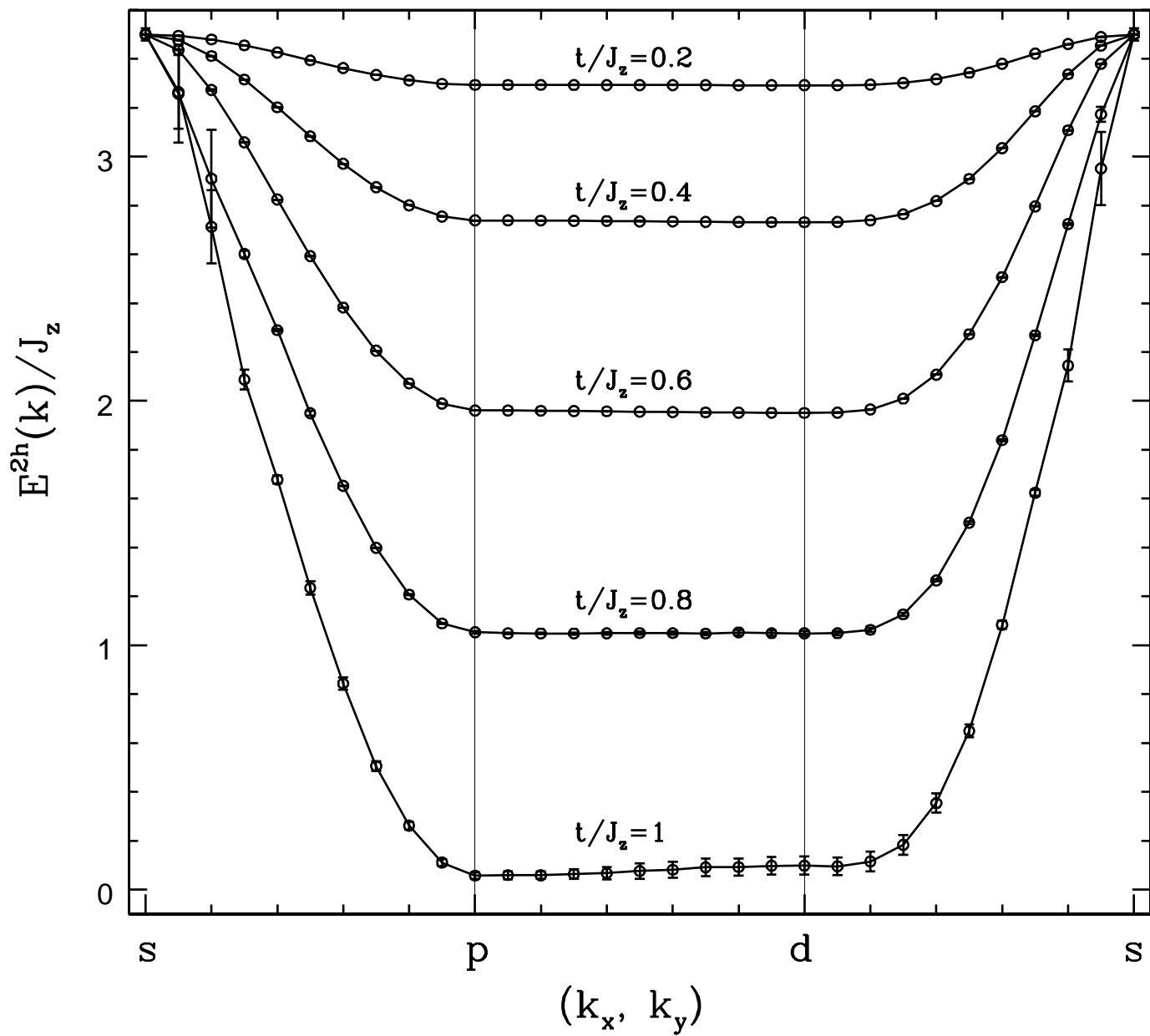
(b)

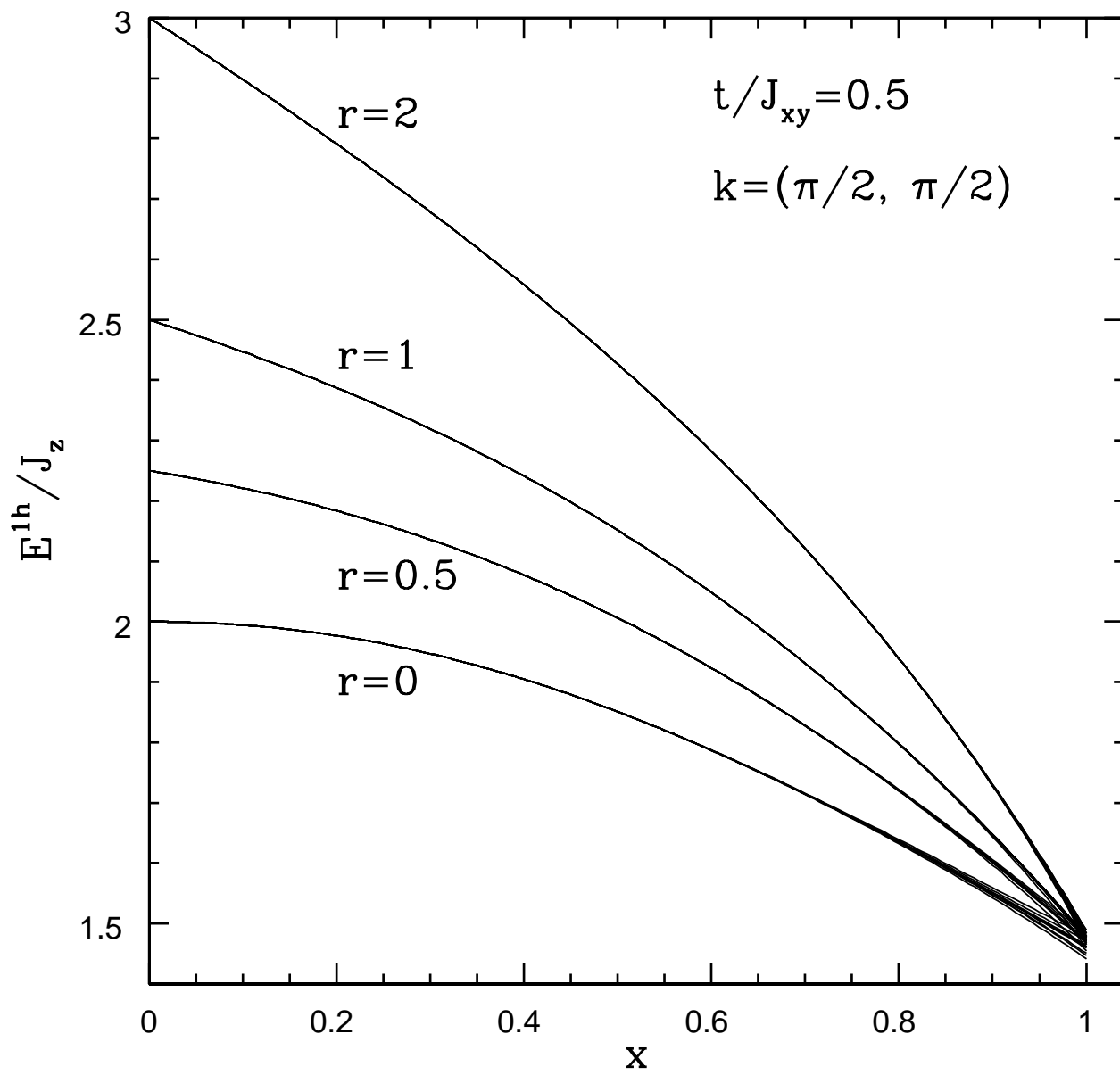


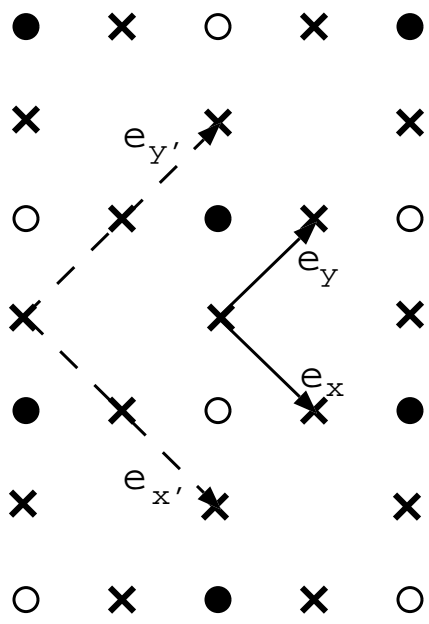




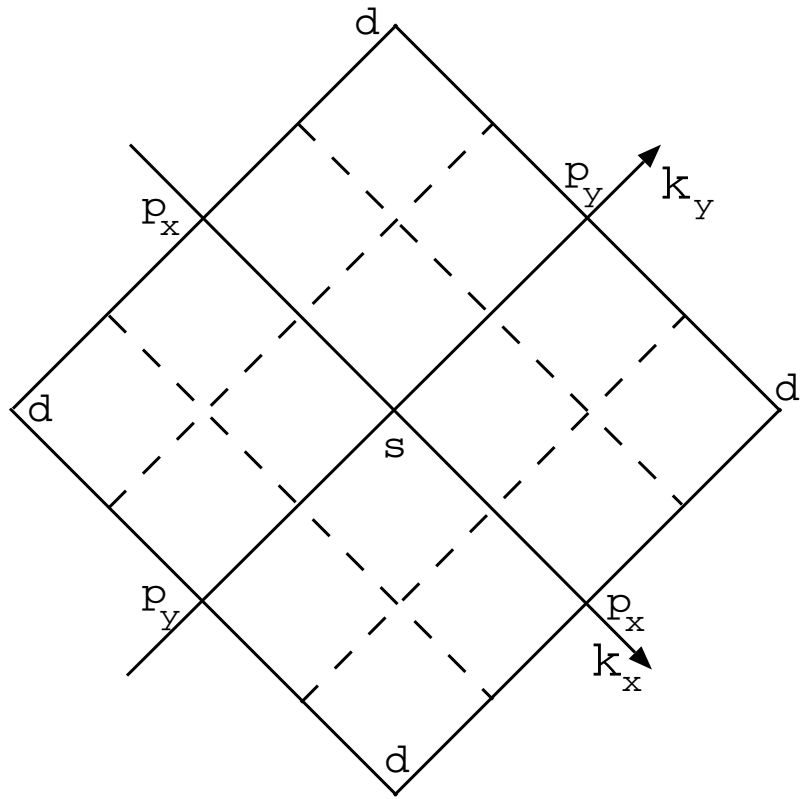








(a)



(b)

